Molecular Biology of the Cell
Vol. 15, 2568–2579, June 2004

A Point Mutation in the Motor Domain of Nonmuscle Myosin II-B Impairs Migration of Distinct Groups of Neurons

Xuefei Ma,* Sachiyo Kawamoto,* Yoshinobu Hara,† and Robert S. Adelstein*‡

*Laboratory of Molecular Cardiology, National Heart, Lung, and Blood Institute, National Institutes of Health, Bethesda, Maryland 20892; and †Neurodevelopment Institute, Sagamihara, Japan 229-1106

Submitted November 24, 2003; Revised February 23, 2004; Accepted March 2, 2004
Monitoring Editor: Thomas Pollard

We generated mice harboring a single amino acid mutation in the motor domain of nonmuscle myosin heavy chain II-B (NMHC II-B). Homozygous mutant mice had an abnormal gait and difficulties in maintaining balance. Consistent with their motor defects, the mutant mice displayed an abnormal pattern of cerebellar foliation. Analysis of the brains of homozygous mutant mice showed significant defects in neuronal migration involving granule cells in the cerebellum, the facial neurons, and the anterior extramural precerebellar migratory stream, including the pontine neurons. A high level of NMHC II-B expression in these neurons suggests an important role for this particular isoform during neuronal migration in the developing brain. Increased phosphorylation of the myosin II regulatory light chain in migrating, compared with stationary pontine neurons, supports an active role for myosin II in regulating their migration. These studies demonstrate that NMHC II-B is particularly important for normal migration of distinct groups of neurons during mouse brain development.

INTRODUCTION

Conventional myosin II, together with actin, comprises the basic contractile machinery involved in a number of cellular processes, including muscle contraction, cytokinesis (De Lozanne and Spudich, 1987), and cell migration (Svitkina *et al*., 1997). Myosin IIs can be broadly divided into muscle-specific isoforms, including skeletal, cardiac, and smooth muscle isoforms, and the ubiquitously expressed nonmuscle isoforms, which are present in most eukaryotic cells, including muscle cells. Both muscle-specific and nonmuscle myosin IIs are made up of a pair of heavy chains (200 kDa) and two pairs of light chains (20 and 17 kDa for nonmuscle and smooth muscle myosins), and it is the heavy chains that have given rise to the names of the nonmuscle myosin: II-A, II-B, and II-C. These nonmuscle myosin heavy chains (NMHCs) are encoded by different genes, and although most cells contain mixtures of these myosins, neurons are in general enriched in NMHC II-B. The expression of all three myosins seems to be regulated in a tissue-specific and developmentally controlled manner (Kawamoto and Adelstein, 1991; Golomb *et al*., 2004).

Article published online ahead of print. Mol. Biol. Cell 10.1091/mbc.E03–11–0836. Article and publication date are available at www.molbiolcell.org/cgi/doi/10.1091/mbc.E03–11–0836.

‡ Corresponding author. E-mail address: adelster@nhlbi.nih.gov.

Abbreviations used: AES, anterior extramural precerebellar migratory stream; DCC, Deleted in Colorectal Cancer; E, embryonic day; EGL, external germinal layer; ES cell, embryonic stem cell; H&E, hematoxylin and eosin; IGL, internal granular layer; ML, molecular layer; NMHC II-B, nonmuscle myosin heavy chain II-B; P, postnatal day; RMLC-P, phosphorylated 20-kDa regulatory myosin light chain.

Proper neuronal migration is critical to the development of the central nervous system. Immature neurons generated from germinal regions migrate to their final destinations where they establish appropriate synaptic connections (for review, see Hatten, 1999). Neuronal migration occurs in two modes, radial and tangential migration. In radial migration, neurons migrate along radial fibers that are perpendicular to the germinal layer. This form of migration occurs throughout the brain, including in the cerebrum and cerebellum. In tangential migration, most neurons migrate attached to one another or to axons instead of to radial glial fibers. Most inhibitory interneurons, some cranial motor neurons, precerebellar neurons, and olfactory granule cells use the tangential mode of migration.

The molecular motors driving neuronal migration are still not fully understood. Molecular and genetic analyses have demonstrated that the actin cytoskeleton and microtubule systems are involved in neuronal migration (for review, see Gleeson and Walsh, 2000). Nonmuscle myosin II is one of the major contributors to the cytoskeleton of neural cells, and its involvement in regulating neuronal migration has been proposed (Wylie and Chantler, 2003), although there is a paucity of direct evidence by using intact brain tissue. A role for myosin II-B has also been demonstrated in the motility of growth cones (Diefenbach *et al*., 2002; Brown and Bridgman, 2003).

Previous work has demonstrated that a null mutation of NMHC II-B resulted in mouse lethality during embryonic development (Tullio *et al*., 2001). Moreover, development of a severe, progressive hydrocephalus, which began to occur at embryonic day 12.5 (E12.5), destroyed the integrity of the brain structure and limited detailed investigation of NMHC II-B function.

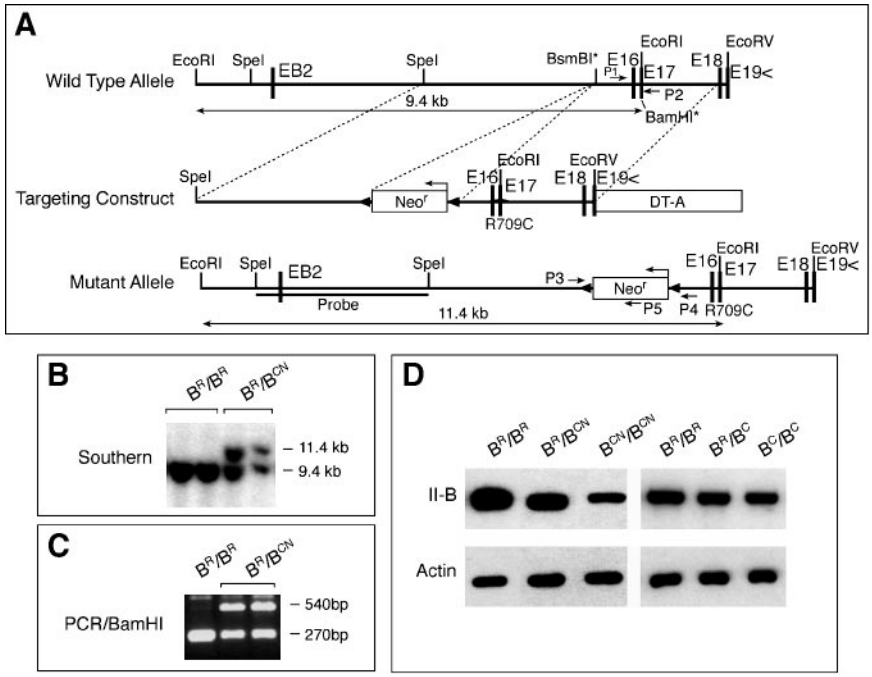

Figure 1. Generation of hypomorphic NMHC II-B R709C mutant mice. (A) Diagram of the wild-type and R709C mutant NMHC II-B allele and targeting construct. The R709C mutation was generated by changing the coding sequence CGG (Arg) to TGC (Cys) in exon 17 (E17). The mutation destroyed a *Bam*HI recognition site in the wild-type allele in E17 (*Bam*HI*). A floxed Neo^r cassette was inserted at the BsmBI* site upstream to the mutation for positive selection. The Diphtheria Toxin-A cassette (DT-A) was placed at the 3′ end of the construct for negative selection. (B) Southern blot analysis of genomic DNA obtained from ES cell clones. Genomic DNA was digested with *Eco*RI and probed with the indicated *Spe*I/*Spe*I fragment (A). Two bands at 11.4 and 9.4 kb represent the targeted (with Neo-cassette) and wild-type allele, respectively. (C) PCR screen of Southern positive ES cell clones. PCR products of genomic DNA amplified by primers p1 and p2 (A) were digested by *Bam*HI to yield fragments of 270 bp (wild-type) and 540 bp (mutant). (D) Western blot analysis of the protein extract obtained from hypomorphic and nonhypomorphic mutant and wild-type mouse brains. The presence of Neo^r in B^{CN}/B^{CN} mice resulted in a 73% reduction in the expression of mutant NMHC II-B compared with wild-type NHMC II-B in B^R/B^R mice (left). Removal of Neo^r restored the expression of the mutant II-B in B^C/B^C mice to the same level as the wild-type II-B in B^R/B^R mice (right). Actin staining is included as a loading control.

To better define a role for NMHC II-B in brain development and to generate a possible mouse model for human disease, we chose to mutate a single amino acid residue in the myosin motor domain (Arg-709 was replaced by Cys, R709C). We selected this residue because R709 and the surrounding residues are conserved in all myosin IIs, suggesting their importance in myosin II function. Moreover, the equivalent mutation was already known to exist for NMHC II-A in humans, generating defects in a number of tissues, including blood cells and kidneys (Heath *et al*., 2001). In addition, baculoviral expression of NMHC II-A heavy meromyosin showed that the equivalent R702C mutation resulted in about a threefold reduction of both the actin-activated MgATPase activity and in vitro translocation of actin filaments (Hu *et al*., 2002).

We now report that R709C NMHC II-B homozygous mice show significantly retarded migration of the facial neurons, cerebellar granule cells, and the anterior extramural precerebellar migratory stream (AES), which includes the pontine neurons and the reticular neurons of the pons. In the case of the cerebellar and pontine neurons, these abnormalities result in a marked ataxia and inability of the pups to maintain proper balance. Our results demonstrate that NMHC II-B is critical for the migration of distinct groups of neurons in the developing mouse brain.

MATERIALS AND METHODS

Gene Targeting and Generation of NMHC II-B R709C Mutant Mice

A brief description of this method in relation to the cardiac defects has been published previously (Takeda *et al*., 2003). A 6.5-kb *Spe*I-*Eco*RV genomic fragment containing exon 17 and surrounding regions of the NMHC II-B gene obtained from a 129/Sv mouse genomic library (Stratagene, La Jolla, CA) was selected for targeting vector construction (Figure 1A). The point mutation R709C was introduced in exon 17 by replacing coding sequence CGG(R) with TGC(C) via recombinant polymerase chain reaction (PCR). Introduction of the R709C mutation destroyed a *Bam*HI site. A floxed Neo^r cassette was inserted into the unique BsmBI site located in an intron 0.9 kb 5′ upstream of the mutation in a 3′-5′ orientation. The Diphtheria Toxin-A cassette was inserted at the 3′ end of the construct for negative selection. The linearized plasmid was electroporated into CMT-1 embryonic stem (ES) cells (Specialty Media, Division of Cell and Molecular Technologies Inc., Phillipsburg, NJ) and selected with G418. Genomic DNA was isolated from the ES cells, digested with *Eco*RI, and hybridized with a 5′ external probe from a *Spe*I-*Spe*I fragment indicated in Figure 1A. Positive clones (Figure 1B) were further screened by *Bam*HI digestion of the PCR products by using primers 1 and 2, which flanked the mutant site (Figure 1A). Heterozygous ES cell clones containing the R709C mutation had one allele resistant to *Bam*HI digestion (Figure 1C). After final confirmation of the mutation by sequencing, three heterozygous ES cell clones were injected into blastocysts derived from C57BL/6 mice. All three clones gave rise to chimeric mice that transmitted the targeted allele into the germline. Mice were maintained in 129/SvXC57BL/6 background for phenotype analysis. Genotyping of progeny was carried out by Southern blot as described above or three-primer PCR (by using primers P3, P4, and P5; Figure 1A) of tail DNA. Mutagenesis was further confirmed in mice by sequencing. To remove the floxed Neo^r cassette, B^R/B^{CN} mice were crossed with mice expressing Cre-recombinase under control of the cytomegalovirus promoter (Balb/C CMV-Cre; The Jackson Laboratory, Bar Harbor, ME). All procedures were conducted using an approved animal protocol in accordance with National Heart Lung, and Blood Institute Animal Care and Use Committee. Immunoblot analyses were carried out on mouse brain samples as described previously (Phillips *et al*., 1995).

Histology and Immunofluorescence Staining

For histology, the samples were fixed with Bouin's fixative overnight at room temperature, and 5-μm-thick paraffin sections were prepared and stained with hematoxylin and eosin (H&E) for microscopic analysis. The embryos were collected in phosphate-buffered saline (PBS) and directly immersed in fixative. The brain was exposed by partial removal of the skin and skull and then fixed by immersion into the fixative. For preparation of brains from mice older than P5, mice were slowly perfused with Bouin's fixative through the left ventricle with an incision in the right atrium. The brains were then dissected out from the skull and immersed in the same fixative. For immunofluorescence staining, samples were manipulated as described for histology, except they were fixed with 4% paraformaldehyde in PBS (pH 7.4) at 4°C. Paraffin sections were then prepared at a thickness of 5 μm. For antibody staining, samples were blocked with PBS containing 0.1% bovine serum albumin/5% normal goat serum for 1 h at room temperature; incubated with polyclonal antibodies against NMHC II-A (1:1000), II-B (1:3000), and II-C (1:1000, Phillips *et al*., 1995; Buxton *et al*., 2003), Hoxb1 (1:200; Covance Research Products, Berkeley, CA), Phox2b (1:500; CeMines Inc., Evergreen, CO), glial fibrillary acidic protein (1:500 dilution; DakoCytomation, Glostrup,

Denmark), monoclonal anti-phospho-regulatory myosin light chain (RMLC) (1:50; Matsumura *et al*., 1998) overnight at 4°C; followed by incubation with fluorescein isothiocyanate-conjugated goat anti-rabbit or goat anti-mouse IgG (1:200; Jackson ImmunoResearch Laboratories, West Grove, PA) for 1 h at room temperature. Instead of specific antibody, normal rabbit or mouse IgG was applied for negative control. After washing, the coverslips were mounted using a Prolong antifade kit (Molecular Probes, Eugene, OR). The images were collected using an SP confocal microscope (Leica, Wetzlar, Germany).

5′-Bromo-2′-deoxyuridine (BrdU) Labeling

To evaluate migrational behavior of cerebellar granule cells in vivo, a single dose (50 μg/g body weight) of the thymidine analog BrdU was injected into P6 littermates. Animals were sacrificed 24 or 72 h after injection, and brains were fixed with paraformaldehyde as described above. BrdU incorporation was detected using a BrdU in situ detection kit (BD Biosciences, San Jose, CA), and slides were counterstained with hematoxylin. To follow migration of the pontine neurons, a single dose of BrdU was injected into pregnant dams at E14.5; the embryos were collected at E16.5 and analyzed for distribution of BrdU-positive pontine migratory cells.

Microexplant Culture of Postnatal Cerebella

Explant cultures were prepared as described by Komuro and Rakic (1996). Cerebella obtained from P0 mice were placed in ice-cold PBS and freed from meninges and choroid plexus. Rectangular pieces (50–100 μm) were dissected from the cerebellar gray matter by using a dissecting microscope. The microexplants were then cultured on a poly-L-lysine/laminin-coated surface in culture medium containing minimal essential medium (Invitrogen, Carlsbad, CA) supplemented with 10% fetal calf serum, 30 mM glucose, 1.8 mM glutamine, 24 mM $NaHCO_3$, 90 U/ml penicillin, and 90 μg/ml streptomycin. To analyze migration of granule cells in culture, phase contrast images of explants were collected between 30 and 66 h at 12-h intervals, and the distance from the edge of explants to the front wave of the migrating cell bodies was measured at each time point. The average rate of granule cell migration was obtained by linear regression analysis. Student's *t* test was used to compare the results between mutant and wild-type littermates. Distribution of myosin II-B in migrating granule cells was visualized by immunofluorescence staining as described above.

RESULTS

R709C point mutant mice were generated by replacing the coding sequence CGG(R) with TGC(C) in exon 17 of NMHC II-B by using homologous recombination (Figure 1, A–C; see MATERIALS AND METHODS). The presence of the Neo^r cassette in the targeted allele resulted in decreased mutant NMHC II-B expression (Figure 1D, left three lanes; cf. B^R/B^R and B^{CN}/B^{CN}, where B^R indicates the wild-type allele and B^{CN} indicates the mutant allele with Neo^r). Removal of the floxed Neo^r cassette by crossing B^R/B^{CN} mice with mice expressing Cre recombinase eliminated the hypomorphic expression as shown in Figure 1D (right three lanes, B^C indicates the mutant allele without Neo^r). The B^{CN}/B^{CN} mice were born at a slightly lower than expected Mendelian frequency. Most of the mice died within the first 2 d after birth. Less than 10% survived up to postnatal day 15 (P15), but one mouse survived to P20. These mice suffered from severe growth retardation by P3 and a progressive hydrocephalus (Figure 2A). Brains dissected from these mice at P12 showed a distorted cerebral cortex and small underdeveloped cerebellum compared with their wild-type littermates (Figure 2B). These mice also developed an early postnatal ataxia manifested as a wide gait (Figure 2A) and frequent loss of balance. To further characterize their balance capability, we attempted to test these mice by using a rotorod (Crawley, 2003). Unlike control littermates, they could not balance on the rotorod at all. Heterozygous mice (B^R/B^{CN}) survived to adulthood without any obvious abnormalities. However, B^C/B^C mice, which expressed increased amounts of mutant NMHC II-B compared with B^{CN}/B^{CN} mice, only survived to embryonic day 16.5 (E16.5). The increased morbidity seen in these mice reflected the increased amounts of mutant myosin expressed, which may act as a dominant negative myosin II with respect to the other myosins. Due to the early embryonic lethality of B^C/B^C mice, we focused our studies here on migration abnormalities of neural cells in B^{CN}/B^{CN} mice. In general, the brain abnormalities described below were also seen in B^C/B^C mice except for the cerebellar defects, which could not be demonstrated in these mice, because they died during embryonic development. Thus, with respect to brain development, the B^{CN}/B^{CN} hypomorphic mutant mice were much more informative. For each phenotype described below, we examined a minimum of five B^{CN}/B^{CN} mice and at least an equal number of B^R/B^R and B^R/B^{CN} littermates generated from two different ES cell clones. The defects described in this article were always observed in the B^{CN}/B^{CN} mice.

Abnormal Foliation of the Cerebellum in Mutant Mice

The nature of the ataxia seen in B^{CN}/B^{CN} mice suggested that cerebellar function was impaired in these mutant mice. This prompted us to analyze cerebellar development during E13.5 to P8. In addition to the small size, the mutant mice displayed marked and consistent abnormalities in cerebellar foliation compared with their wild-type littermates (Figure 2, E–H). At E13.5, the cerebellar primordium formed with no obvious difference in the mutant embryos compared with the wild-type littermates (Figure 2, C and D). However, in newborn mutants (P0), the fissures were shallower than in wild-type littermates, and some of them, such as between folia II and III, and VII and VIII, were not even formed (Figure 2F, arrowheads). By P8, wild-type mice developed a mature foliation pattern within the vermis, with characteristic folia separated by well-defined fissures. In the mutant mice, fissures in the posterior portion of the cerebellum (folia VIII-X) looked almost normal, but those in the middle and anterior portions were defective and either seemed shallower or were missing (Figure 2H, arrowheads). The abovementioned findings suggested that the abnormal foliation in the mutant mice was not the result of the smaller size of these mice and/or a delay in development.

Abnormal Layer Formation in the Mutant Cerebellum

The cerebellar cortex forms a characteristic layered structure during normal development through the cooperative interactions between cerebellar Purkinje cells and granule cells. To further identify developmental defects in the mutant cerebellum, we analyzed the process of layer formation during postnatal development (Figure 3, A–F). During normal development of the cerebellar cortex, the thickness of the external germinal layer (EGL) increases, starting from P0 due to the proliferation of granule cell precursors and reaches a maximal thickness around P8 (Figure 3C). The EGL then decreases and almost disappears by P15 (Figure 3E). On the other hand, the internal granular layer (IGL) increases its thickness continuously throughout this period, due to the migration of postmitotic granule cells from the EGL. At P0, the EGL was slightly thinner in the mutant mice compared with their wild-type littermates (Figure 3, A and B). In contrast, by P8, striking defects were observed in mutant mice. Although thickness of the EGL was comparable between mutant and wild-type mice, the IGL of the mutant mice was only one-half the thickness of the wild-type IGL (Figure 3, C and D). By P15, the EGL was still more prominent in mutant mice than in the wild-type mice, and although the thickness of the mutant IGL was increased, it still lagged behind the wild type (Figure 3, E and F). Thus, both the rate of decrease in the thickness of the EGL and the rate of increase in the thickness of IGL took significantly longer in mutant mice compared with their wild-type litter-

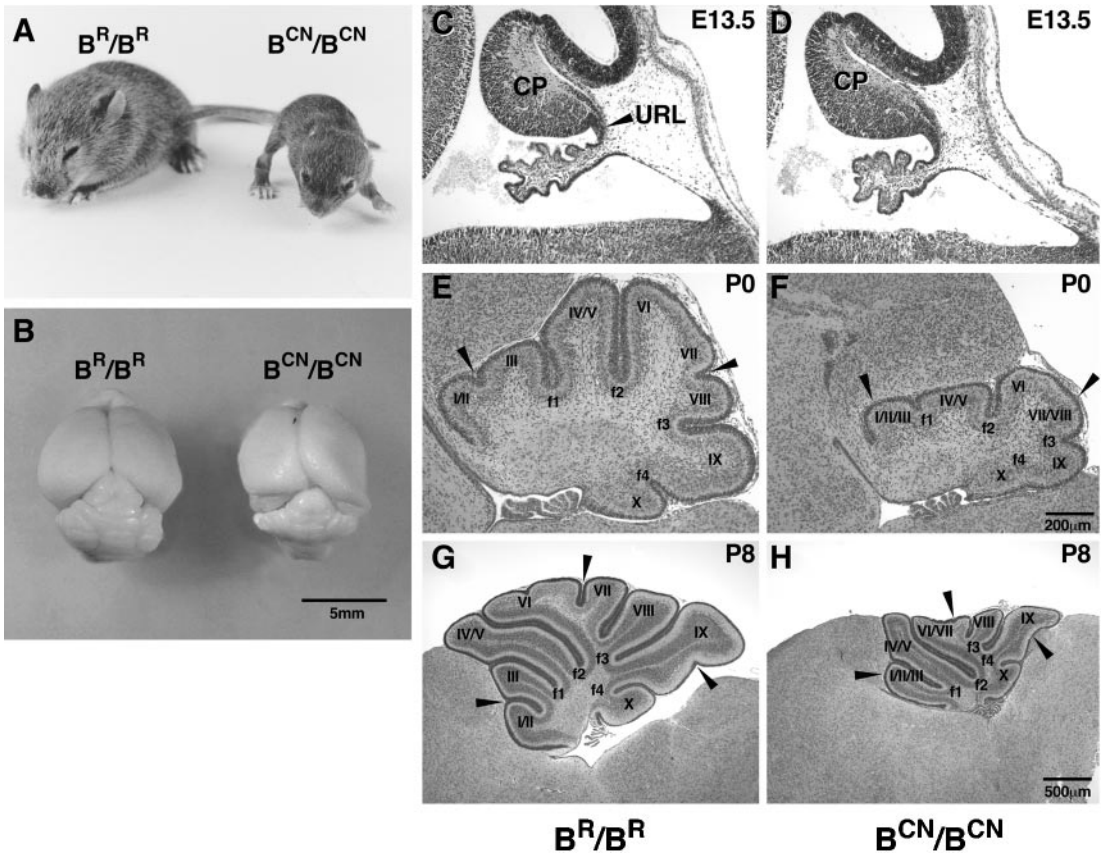

Figure 2. Motor dysfunction and abnormal cerebellar foliation in mutant mice. (A) Picture of a P15 R709C homozygous mutant (B^{CN}/B^{CN}) mouse and wild-type littermate (B^R/B^R). The B^{CN}/B^{CN} mouse shows severe growth retardation, progressive hydrocephalus and a broad-based gait compared with wild-type littermate. (B) Gross view of the brains of B^{CN}/B^{CN} and B^R/B^R mice. The B^{CN}/B^{CN} mouse brain shows a distorted cerebral cortex due to hydrocephalus and an underdeveloped cerebellum. (C–H) Midsagittal cerebellar sections of mouse brains at the ages indicated stained with H&E. No obvious differences in the formation of the cerebellar primordium (CP) are found in the mutant mice (B^{CN}/B^{CN}) compared with the wild-type littermate (B^R/B^R) at E13.5 (C and D). E–H demonstrate the impaired cerebellar foliation pattern with missing fissures in the mutant mice (cf. arrowheads in F with E at P0, and H with G at P8) compared with the wild-type littermates. URL, upper rhombic lip.

mates, suggesting a decrease in the rate of migration of granule cells in the mutant mice. Consistent with this idea, a reduced number of migrating granule cells was seen in the molecular layer of the mutant mice compared with their wild-type littermates (Figure 3, C and D, arrows). At P8, the average number of migrating granule cells in the molecular layer of wild-type mice was $71 \pm 3/mm^2$, compared with 27 ± 2 for the mutant mice ($p < 0.0001$, $n = 4$ mice).

Impaired Migration of Cerebellar Granule Cells In Vivo

To investigate whether migration of cerebellar granule cells was affected in B^{CN}/B^{CN} mutant mice, we labeled dividing cells at P6 with BrdU and followed migration of these cells for 3 d by using antibodies to detect BrdU (Figure 3, G–J). The proliferating cells in the EGL took up BrdU during the cell cycle. Only the postmitotic granule cells that exited the cell cycle, which were strongly labeled with BrdU, migrated toward the IGL, whereas the other cells that entered into the next cycle diluted their BrdU label. Note that approximately the same number of granule cells was labeled with BrdU in the B^R/B^R and B^{CN}/B^{CN} mice. Examination of the more heavily labeled granule cells 24 h after labeling showed that in the wild-type mice, some BrdU-labeled granule cells were found in the molecular layer (ML) and IGL, but most of them were localized in the premigratory zone of the EGL (Figure 3G, arrowhead). At 72 h after labeling, however, the majority of the wild-type–labeled granule cells were found in the IGL, with only a few of them remaining at the edge of the EGL and in the ML (Figure 3I). In contrast, in mutant mice there was a slower transfer of the labeled cells from the proliferative zone to the premigratory zone at 24 h, with most of the BrdU-labeled cells still localized in the proliferative zone (Figure 3H). At 72 h, more of the BrdU-labeled granule cells were found in the IGL; however, many of them were still present within the premigratory zone (Figure 3J). Quantification of BrdU-positive cells showed that at 24 h, $93 \pm 3\%$ of these cells were located in the EGL of wild-type mice and $91 \pm 6\%$ in the mutant EGL, whereas at 72 h, only $8 \pm 2\%$ remained in the EGL of wild-type mice and $52 \pm 10\%$ remained in the B^{CN}/B^{CN} mice ($n = 3$ mice). The delayed granule cell migration from the EGL also explained the thinner molecular layer seen at P8 and P15 in the mutant mice, because the granule cells were delayed in spinning their parallel fiber axons.

During cerebellar development, granule cells migrate from the EGL to the IGL along Bergmann glial fibers. It is possible that a mutation at R709C in NHMC II-B could affect the Bergmann glial fiber system and consequently alter

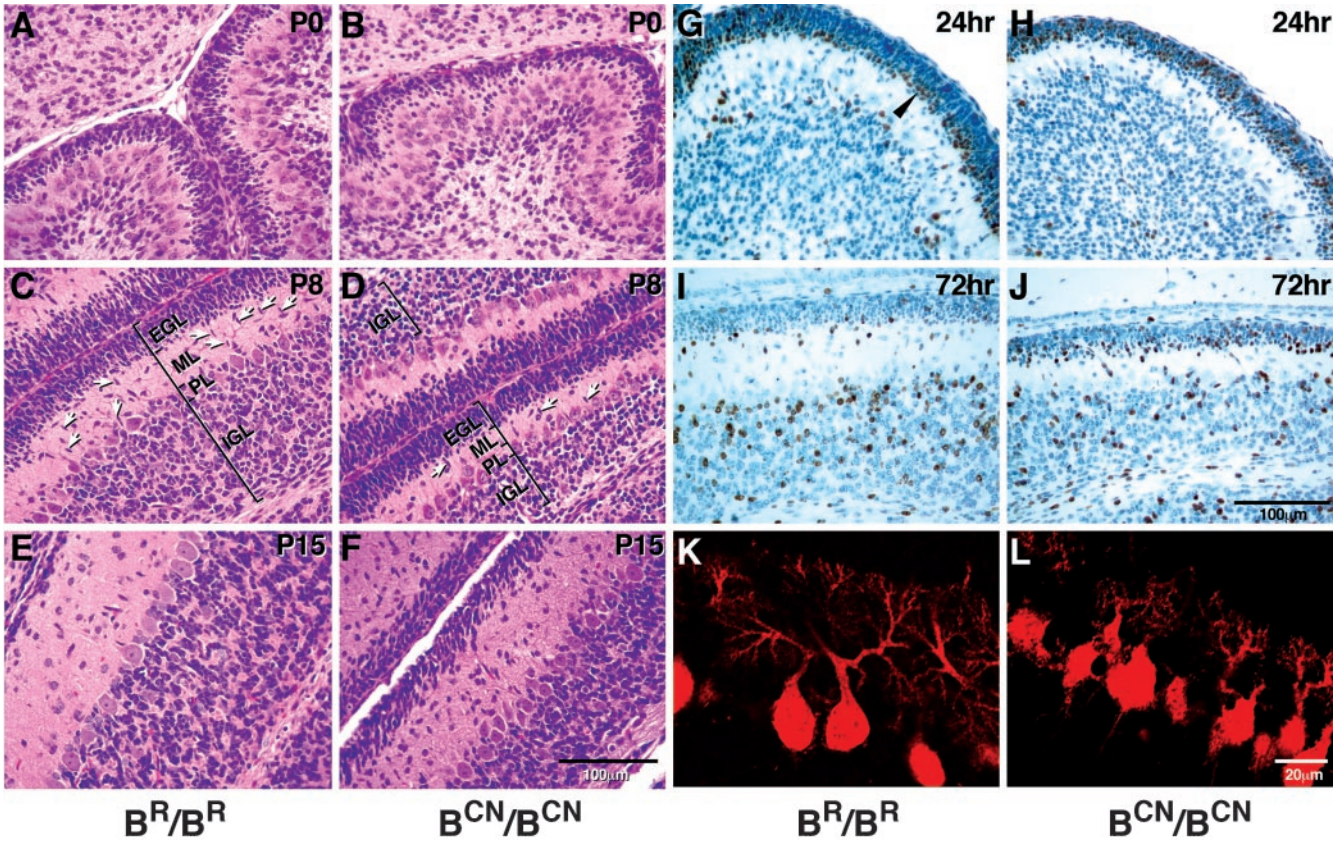

Figure 3. Abnormal layer formation in the mutant cerebellum. (A–F) Midsagittal cerebellar sections of mouse brains at ages indicated stained with H&E. At P0, a small decrease in the thickness of the external germinal layer (EGL) of the cerebellum is evident in B^{CN}/B^{CN} mice (B) compared with that in B^{R}/B^{R} mice (A). At P8, the mutant EGL is similar in thickness to the wild-type, but the IGL is only about one-half the size of the wild-type (cf. the mutant D with wild-type C). A decreased number of migrating granule cells is also found in the ML in mutant mice compared with wild-type mice (arrows). At P15, the EGL of the mutant cerebellum is thicker than the wild-type and the mutant IGL remains thinner than the wild-type (cf. the mutant F with wild-type E). (G–J) Sagittal sections of mouse cerebellum immunostained for BrdU and counterstained with hematoxylin. BrdU was injected at P6. BrdU-positive postmitotic granule cells (brown staining) are localized to the premigratory zone of the EGL 24 h after injection (G, arrowhead), and most of them have migrated to the IGL by 72 h in wild-type (B^{R}/B^{R}) mice (I). However, in the mutant (B^{CN}/B^{CN}) mice, many BrdU-positive cells are located throughout the EGL 24 h after injection (H), and many of these cells are still found in the EGL at 72 h, although most have now accumulated in the premigratory zone (J). (K and L) Confocal immunofluorescent microscopic images of the sagittal sections of P8 mouse cerebellum stained with antibody against calbindin showing dendritic trees and cell bodies of the Purkinje cells. The B^{CN}/B^{CN} mice show underdeveloped Purkinje cells with less arborization and stunted dendritic trees (L) compared with B^{R}/B^{R} mice. PL, Purkinje cell layer.

granule cell migration. To visualize the glial fibers, we stained sections with an antibody against glial fibrillary acidic protein. The glial processes were observed to run through the whole developing molecular layer and external granule layer in both the mutant and wild-type mice. To examine whether the mutant granule cells exhibit enhanced apoptotic activity, which could also contribute to abnormal layer formation, we carried out a terminal deoxynucleotidyl transferase dUTP nick-end labeling assay by using cerebellar sections obtained from the mutant and wild-type mice at P8. No differences were observed in the extent of apoptosis between the two groups of mice (our unpublished data).

In addition to the defects in granule cell migration, impaired development of cerebellar Purkinje cells was also seen in the mutant mice. The cell bodies of the mutant Purkinje cells were small and not aligned as regularly as the wild-type cells (Figure 3, D and F). The average width and height of the Purkinje cell body in wild-type mice was 53 ± 0.7 and 88 ± 1 μm, respectively, and 51 ± 0.6 and 78 ± 1 μm for the mutant mice ($p < 0.001$, $n = 4$ mice). Moreover, immunostaining of tissue sections with antibodies raised against calbindin showed a stunted dendritic tree with fewer branches compared with the normal cells (Figure 3, K and L).

Slowed Migration of Cerebellar Granule Cells in Microexplant Cultures from Mutant Mice

Both histological analyses and an in vivo migration assay pointed to a migrational defect in the cerebellar granule cells of NMHC II-B mutant mice. To further explore this possibility, we carried out an in vitro migration assay by using microexplant cultures. Cerebellar microexplants were dissected from P0 mice, both from mutant and wild-type littermates and cultured on a poly-L-lysine/laminin-coated surface. Granule cell migration was monitored between 30 h and 66 h in the explants and evaluated by measuring the distance from the front wave of the migrating cell body to the edge of the explants at different times in culture. Figure 4 shows representative images of explants at different time points in cultures from wild-type (A, C, E, and G) and mutant mice (B, D, F, and H). Both wild-type and mutant

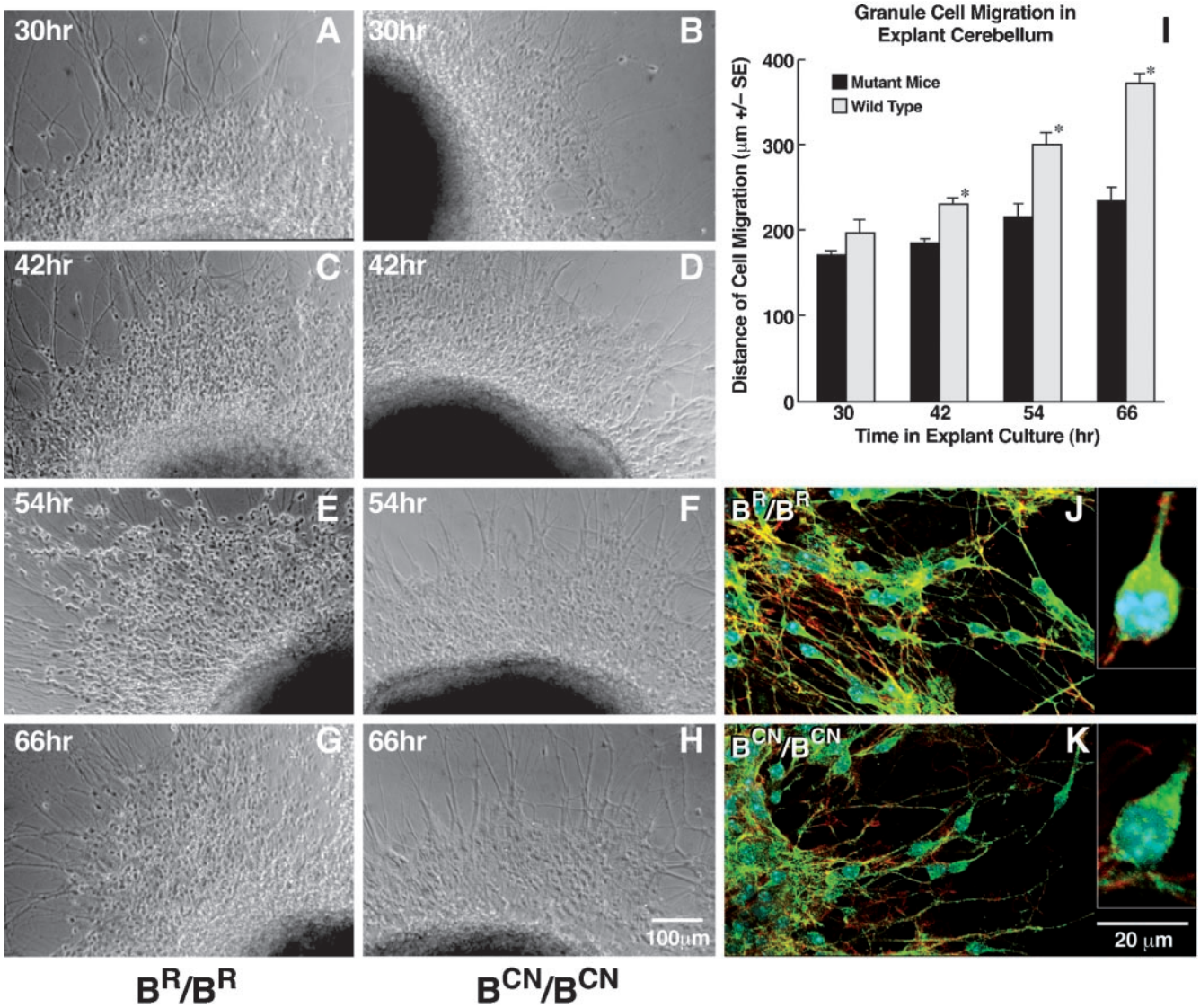

Figure 4. Slowed migration of mutant cerebellar granule cells in microexplant cultures. (A–H) Examples of phase contrast images of the migrating granule cells at indicated times in microexplant cultures from B^R/B^R (A, C, E, and G) and B^{CN}/B^{CN} mice (B, D, F, and H). (I) Bar plot comparing the distance traversed by the front wave of the migrating cell bodies between explants from wild-type and mutant mice, showing a significantly slowed progression of the granule cells from mutant mice (*$p < 0.0001$, $n = 8$). (J and K) Immunofluorescence confocal images. Green indicates NMHC II-B stained with anti-NMHC II-B, red indicates actin stained with rhodamine-phalloidin, blue indicates nuclei stained with 4,6-diamidino-2-phenylindole. Accumulation of NMHC II-B in the perinuclear area of migrating cerebellar granule cells is seen in wild-type mice (J), but it is not consistently seen in the mutant cells (K). Insets in J and K show asymmetric distribution of NMHC II-B in migrating granule cells at high magnification for wild-type and mutant cells.

cells initiated cell migration and extruded long neurites radially. However, the mutant cells migrated significantly more slowly than the wild-type cells (quantitated in Figure 4I). The average rate of migration of the mutant cells was 1.8 μm/h, whereas the average rate for wild-type cells was 4.9 μm/h over the period from 30 to 66 h in culture ($n = 8$). Immunofluorescence confocal microscopy using antibodies raised against NMHC II-B revealed that NMHC II-B was asymmetrically distributed in the leading boundary of the perinuclear region in practically all migrating granule cells of explants obtained from wild-type mice (Figure 4J and inset). This asymmetric distribution of myosin II-B was not consistently seen in cells cultured from B^{CN}/B^{CN} mice, although some (~30%) of the mutant migrating granule cells also showed a similar pattern of staining (Figure 4K and inset).

Delayed Migration of the AES

A second striking abnormality in the B^{CN}/B^{CN} mutant brain indicating abnormal migration of neural cells was suggested by the complete absence of pontine nuclei at their normal destination at P0 (cf. Figure 5, A and D). During mouse brain development beginning from E13, progenitors of the pontine neurons in the caudal portion of the rhombic lip proliferate and migrate toward the ventral midline around the circumference of the neural tube, in a dorsal to ventral trajectory. These cell populations, along with the progenitors of the reticular neurons of the pons form the AES just

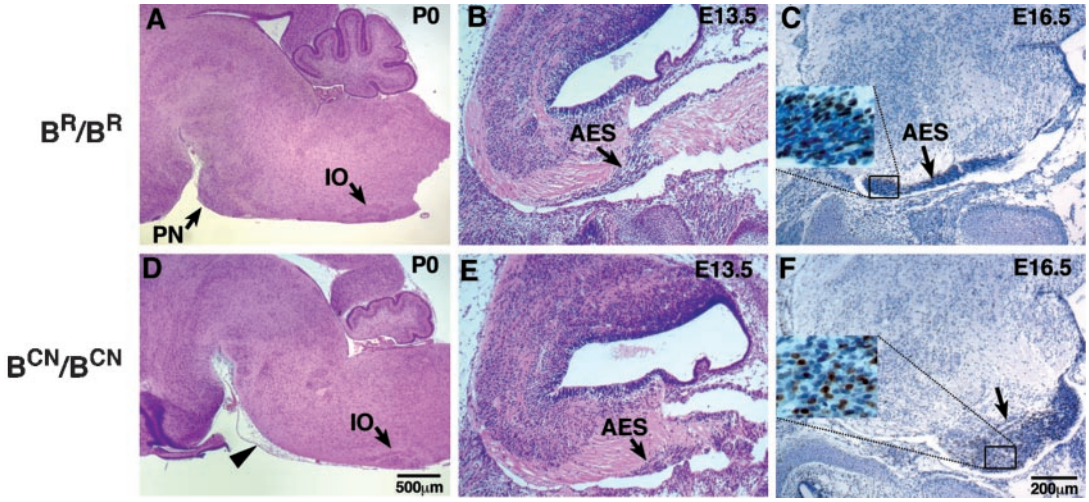

Figure 5. Abnormal migration of the mutant AES. Sagittal sections of mouse brains at indicated ages stained with H&E (A, B, D, and E) or immunostained for BrdU and counterstained with hematoxylin (C and F). Pontine nuclei (PN) are absent at their normal destination in B^{CN}/B^{CN} mice at P0 (D, arrowhead); however, no obvious abnormalities in the formation of the inferior olive (D, IO) are found in these mice. The AES is initiated in mutant mice (E, arrow) similar to wild-type mice (B, arrow) at E13.5. However, defects in the progression of the AES are evident in B^{CN}/B^{CN} mice at E16.5 (F, arrow). The insets in C and F demonstrate the presence of BrdU-labeled neurons (brown staining) in the AES and are enlarged from the indicated areas.

beneath the pial surface (Altman and Bayer, 1987; Altman and Bayer, 1997). In mutant mice, the pontine neurons failed to reach their final destination in the basilar pons.

To analyze how migration of the pontine neurons was disrupted by the NMHC II-B mutation, we first examined whether initiation of migration was delayed in the mutant mice at E13.5. As shown in sagittal sections of brains, a normal AES migrating toward the basilar pons was evident in the mutant animals (Figure 5E), similar to their wild-type littermates (Figure 5B). This suggested that the R709C mutation in NMHC II-B did not disturb the generation of pontine neural cells or initiation of cell migration. We next analyzed the progression of this migration by injecting a single dose of BrdU into pregnant dams at E14.5 and examining BrdU-positive neurons at E16.5. The results at E16.5 showed that in wild-type mice the AES, which included the cells labeled with BrdU, had reached near to the basilar pons where these neurons normally reside (Figures 5C and 9I). In mutant mice, however, the AES did not reach this far, and instead a large group of neurons, including the pontine neurons and the reticular neurons of the pons, accumulated under the pial surface in the lateral posterior area of the medulla (Figure 5F, arrow). Careful examination of serial coronal sections from mouse brains confirmed that the pontine neurons completed their migration and settled at their final destination in wild-type P0 mice (Figure 6, A, C, and E). However, as noted above, almost no pontine neurons were found at their normal destination in mutant mice where, instead, they were localized along the AES in the lateral posterior region of the pons (Figure 6, B, D, and F). Consistent with this, the reticular nuclei of the pons were also absent from their normal location in B^{CN}/B^{CN} mice at P0 (Figure 6, cf. G and H).

Defects in migration of precerebellar neurons were not only confined to the AES, because an abnormal accumulation of the posterior extramural migratory stream, which carries migrating neurons for the lateral reticular and external cuneate nuclei, was also observed in the mutant mice. However, unlike the AES, some of these neurons reached their final destination (our unpublished data). The migration of the posterior intramural migratory stream did not seem to be affected in the mutant mice, because no abnormalities in formation of the inferior olive were seen (Figure 5D).

Abnormal Protrusion of Facial Neurons into the Fourth Ventricle

Scanning of serial coronal sections from B^{CN}/B^{CN} mouse brains at P0 revealed that the facial neurons were greatly diminished in the mutant mice compared with their wild-type littermates (cf. Figure 7, A, C, and E with B, D, and F). Whereas some of the facial neurons located medially (labeled VII*m*) were still observed in the mutant mice, the more lateral facial neurons (VII*l*) were almost all missing in these animals (cf. Figure 7, A and C with B and D). Moreover, in B^{CN}/B^{CN} mice, a mass of neurons, morphologically resembling facial neurons (Figure 7, E and F, insets), was noted to consistently accumulate and protrude into the fourth ventricle near the normal origin of these neurons (Figure 7, B, D, and F, arrowheads). To confirm that the ectopic neurons noted in the area of the fourth ventricle were derived from facial neurons, we analyzed sagittal sections of mouse embryos at E13.5, by which time the facial neurons had almost completed their migration in wild-type mice (Figure 7G). However, in B^{CN}/B^{CN} mutant mice, only a small number of the facial neurons were situated in their normal destination (Figure 7H). A group of large-sized neurons that were not seen in wild-type mice (Figure 7I) were consistently found near the origin of the facial neurons at the recess of the pontine flexure of the fourth ventricle (Figure 7J, arrowhead). We stained sagittal sections of the mutant mouse brain with an antibody against Hoxb1, a transcription factor that marks rhombomere 4-derived neurons (Garel *et al.*, 2000), as well as an antibody against Phox2b, a protein that is highly expressed in facial neurons. As shown in Figure 7, L and N, the ectopically protruded neurons in B^{CN}/B^{CN} mice as well as the facial neurons in wild-type mice (Figure 7, K and M) stained positively for Hoxb1 (Figure 7, K and L) and Phox2b (Figure 7, M and N), confirming the identification of the protruding group of neurons.

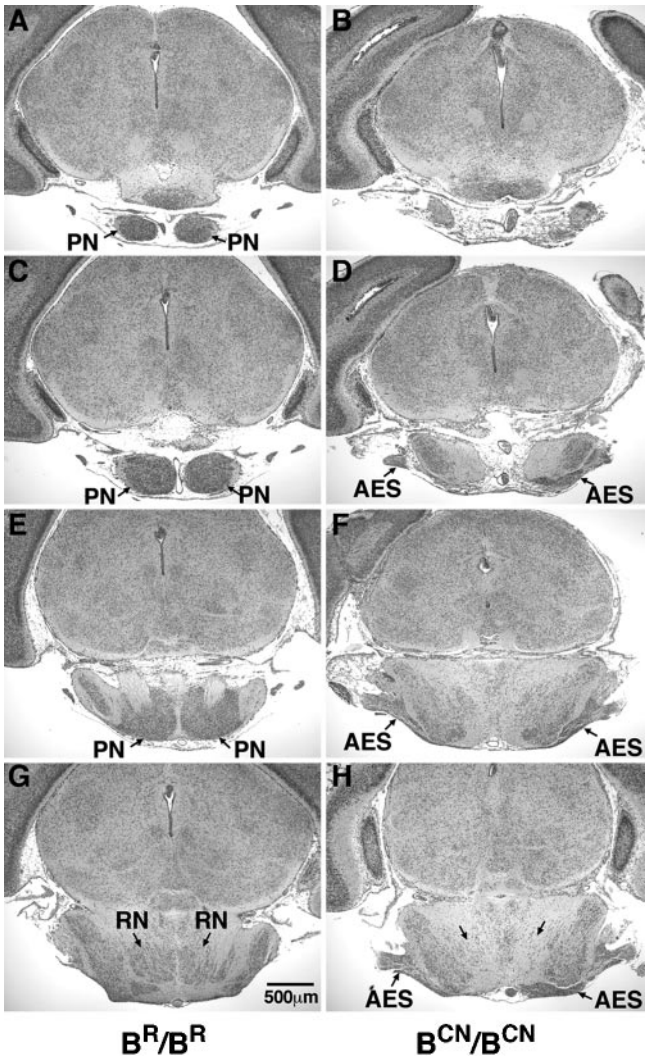

Figure 6. Coronal sections of the abnormal migration of the AES in mutant mice. Serial coronal sections (anterior to posterior) of a P0 mouse brain stained with H&E, showing absence of pontine nuclei (PN) in a B^{CN}/B^{CN} mouse (cf. normal A, C, and E with mutant B, D, and F) and an abnormal accumulation of the AES at the lateral posterior region (D, F, and H, arrows), which is not seen in the wild-type (B^R/B^R) mouse (C, E, and G). Note also that the reticular nucleus of the pons is seen in its normal location in the wild-type mouse (G, RN), but not in the mutant mouse (H, arrows).

Expression of NMHC II-B in Cerebellar Granule Cells, the AES, and Facial Neurons

Although subtle defects in the migration of neural cells were also seen in other regions of the mutant brain, including hippocampus, cerebral cortex, and olfactory bulbs, the most striking defects of neuronal migration were confined to cerebellar granule cells, the AES, and facial neurons. It is intriguing as to why these three groups of neurons were more vulnerable than others. One possibility may lie in differences in expression of the three myosin II isoforms. We therefore examined the pattern of NMHC II-A, II-B, and II-C distribution in the developing brains of wild-type mice by immunofluorescence confocal microscopy by using affinity-purified antibodies raised against NMHC II-A, II-B, and II-C (Figure 8). All three antibodies stained brain structures; however, important differences were observed. Whereas antibodies raised to NMHC II-A strongly stained the vasculature and only weakly stained neural cells (Figure 8, A–D), those raised to II-B and II-C mostly stained neural cells (Figure 8, E–L). Close examination of the premigratory zone of the EGL and the developing Purkinje cells at P8 showed enhanced staining for NMHC II-B compared with NMHC II-B staining of the surrounding neural cells in the same section (Figure 8E). Enhanced expression of NMHC II-B compared with surrounding tissues was also seen in the AES, as well as the facial neurons at E16.5 (Figure 8, F and H, respectively). This enhanced expression of NMHC II-B in the most severely affected neurons was not seen for NMHC II-C, which was uniformly stained in neuronal cells or for NMHC II-A (Figure 8, A–D and I–L). Importantly, neurons of the inferior olive, which did not show an obvious defect in cell migration, also did not show increased expression of NMHC II-B (Figure 8G). These results suggest that normal migration of the AES, facial neurons and cerebellar granule cells relies more on nonmuscle myosin II-B function than does migration of other neural cells such as those present in the inferior olive and that a mutation in the myosin motor domain of these neurons may make them more vulnerable to defects in migration.

Nonmuscle myosin II is activated by phosphorylation of its 20-kDa RMLC on Ser-19 (for review, see Sellers, 1999). To further investigate the possible involvement of nonmuscle myosin II function during neuronal migration, we examined the relative amount of RMLC phosphorylation in migrating and postmigrating pontine neurons of wild-type (B^R/B^R) mice by immunostaining with an antibody specific for the phosphorylated Ser-19 RMLC (RMLC-P; Matsumura *et al.*, 1998). Figure 9 shows the distribution of RMLC-Ps at E16.5 in the AES, which contained the migrating pontine neurons, and at P21, after the pontine neurons had reached their destination. Note the relative increase in the intensity of RMLC-P staining in the migrating neurons in the AES compared with the surrounding area (Figure 9, A and B). In contrast, this difference in intensity was not seen for pontine neurons at P21 when they had ceased migrating (Figure 9C; PN). Only the vasculature, which contained RMLC-Ps associated with smooth muscle and nonmuscle myosin II, showed more intense staining (Figure 9, B and C, arrows). Note that the staining for NMHC II-B in the AES and pontine neurons remained intense compared with the surrounding areas, and in contrast to that for the RMLC-Ps, was unaltered between E16.5 and P21 (Figure 9, E and F, and G) for B^R/B^R mice. (Note that 9E and 8F are the same panel.) With respect to B^{CN}/B^{CN} mice, we found increased staining for both the RMLC-P (Figure 9D, arrowhead) and NMHC II-B (Figure 9H, arrowhead) in a population of neural cells that accumulated beneath the pial surface, most likely the AES. These panels showed that the R709C mutation does not impair the phosphorylation of the RMLC or the regional expression pattern of myosin II-B during the time that it interfered with pontine neuronal migration. The identification of the AES and the pontine neurons was confirmed by H&E staining shown in I–L; M–P are negative controls with the use of normal rabbit IgG as primary antibody.

DISCUSSION

Myosin II-B Regulates Progression of Neurons during Migration

Our experiments demonstrate that during brain development, homozygous mice expressing mutant NMHC II-B show marked abnormalities of migration in certain major groups of neurons: cerebellar granule cells, pontine neurons, reticular neurons of the pons, and facial neurons. Normal migration of neural cells depends on three different cellular

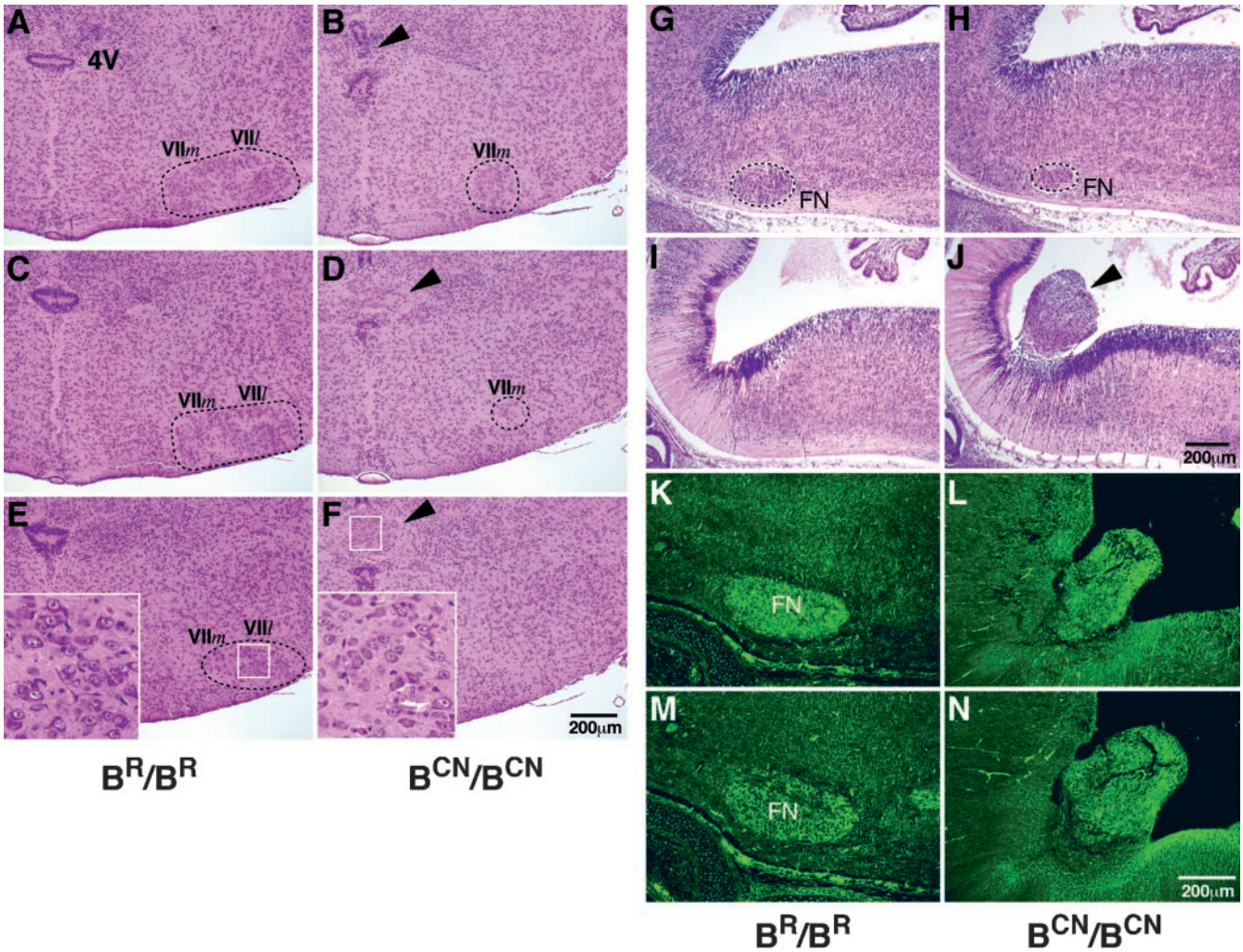

Figure 7. Diminished facial neurons and their abnormal protrusion into the fourth ventricle in mutant mice. (A–F) Serial coronal sections (anterior to posterior) of P0 mouse brains stained with H&E. Diminished facial neurons are evident in B^{CN}/B^{CN} mice (B, D, and F) compared with B^{R}/B^{R} littermates (A, C, and E). Only some medial facial neurons (VII*m*) are observed in the mutant mice, but the lateral facial neurons (VII*l*) are not seen (cf. Band D with A and C). In addition, the fourth ventricle (4V) in B^{CN}/B^{CN} mice is disrupted by an ectopic group of large-sized neurons (B, D, and F, arrowhead) similar to facial neurons of the wild-type mice (cf. inserts in F with E). The white box outlines the region enlarged in the insert. (G–J) Serial sagittal sections (lateral to medial) of mouse brains at E13.5 stained with H&E. At E13.5, facial neurons have just completed their migration. A diminished number of facial neurons (FN) is seen in B^{CN}/B^{CN} mice (H) compared with B^{R}/B^{R} littermates (G). Protrusion of a group of neurons into the fourth ventricle near the region where the facial neurons originate is observed in the mutant mice (J, arrowhead) but not in the wild-type mice (I). (K–N) Sagittal sections of mouse brains at E16.5 immunostained for two different marker proteins showing positive staining of the protruded neurons (L and N) and normal facial neurons (K and M) for both Hoxb1 (K and L) and Phox2b (M and N).

processes: initiation, progression, and stop (for review, see Sobeih and Corfas, 2002). Here, we suggest that NMHC II-B contributes to the progression of neuronal cell migration and that a mutation in NMHC II-B slows the speed of neuronal migration. Impairment in the direction of cell migration could also result in abnormal cell migration. However, this seems not to be the case in our mutant mice because all the affected neurons are located in their normal migrating paths, but they fail to reach their final destination. For example, in NMHC II-B mutant mice, the neurons of the AES fail to reach their normal destination in the ventromedial part of the pons. Instead, they accumulate laterally and posteriorly along their normal migratory trajectory. Whereas normal initiation of the AES is observed in B^{CN}/B^{CN} mice, the progression of the stream is greatly retarded. Migration of the pontine neurons is controlled by guiding signals such as netrin signaling, and loss of pontine neurons also has been reported in netrin knockout mice (Serafini *et al*., 1996). However, the inferior olive, which is also guided by netrin signaling and which is also significantly diminished in netrin knockout mice (Bloch-Gallego *et al*., 1999), is not affected in NMHC II-B mutant mice. Therefore, the guiding signals for migration of the pontine neurons seem to be unaffected in B^{CN}/B^{CN} mice.

Abnormalities in the migration of the facial neurons in the B^{CN}/B^{CN} mice also seem to arise from a defect in the progression of migration. First, some of the facial neurons do reach their final destination, which implicates the existence of proper environmental signaling. Second, most of the mutant facial neurons do not situate randomly; instead, they protrude as a group into the fourth ventricle during their normal migratory passage. Slowed migration of facial neurons may result in

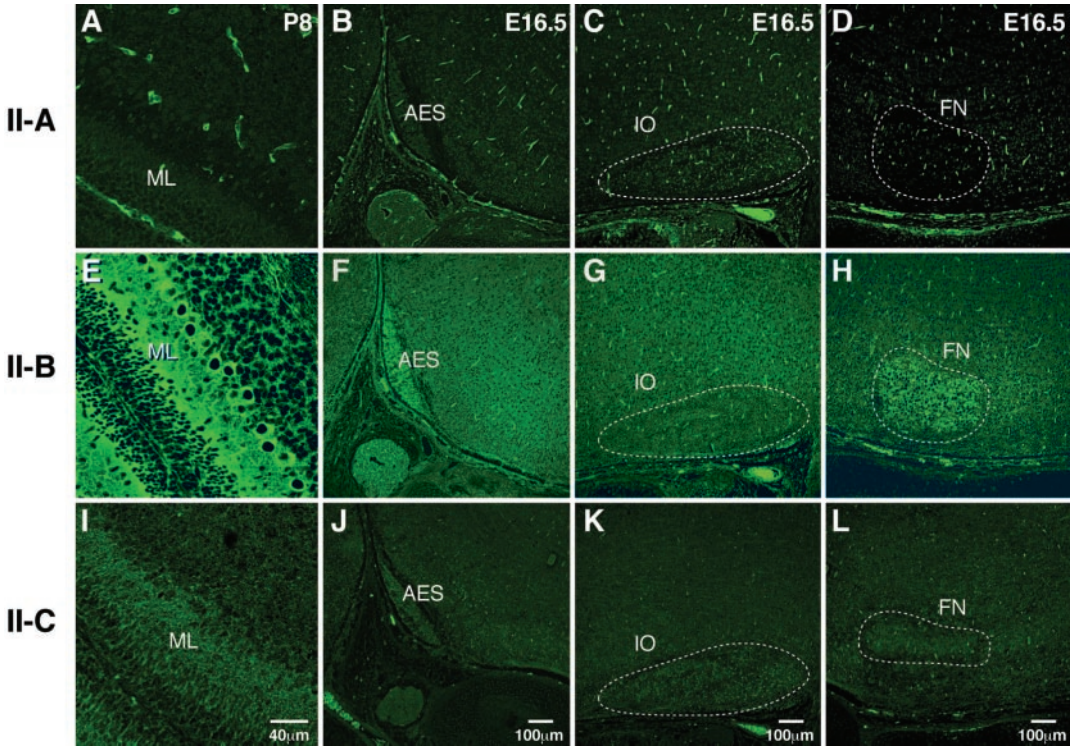

Figure 8. Differential distribution of NMHC II-B in wild-type mouse brain. Immunofluorescence confocal images stained for NMHC II-A (A–D), II-B (E–H), and II-C (I–L) in developing cerebellum (A, E, and I), areas around the AES (B, F, and J), inferior olive (C, G, and K), and facial neurons (D, H, and L). Strong staining of the vasculature is obvious for NMHC II-A (A–D). NMHC II-B is detected throughout the brain, but more intense staining is present in the ML of the developing cerebellum (E), the AES (F), and facial neurons (H, FN). In contrast, neurons of the inferior olive (G, IO) do not show any increased staining with II-B. NMHC II-C is uniformly stained throughout all the brain sections. Negative controls using normal rabbit IgG as the primary antibody did not show fluorescence.

accumulation of the newborn neurons near the origin of these cells, at the recess of the pontine flexure of the fourth ventricle. Accumulation of these neurons may result in their protrusion into the fourth ventricle. An abnormal accumulation of a neural cell mass in the fourth ventricle has also been reported in NMHC II-B null mice (Tullio *et al*., 2001); however, the identity of the neurons was not clear.

Alteration in the migratory behavior of neural cells in NMHC II-B mutant mice is not confined to tangential migration. Radial migration of the cerebellar granule cells from the mutant mice is also significantly affected. Evidence from histological analysis and in vivo assays of granule cell migration demonstrates a slowed migration of cerebellar granule cells in the mutant mice. We postulate that slowed migration of the mutant cerebellar granule cells is the result of a disturbance in their intrinsic migratory machinery. Consequently, the decrease in the thickness of EGL and increase of IGL and ML are delayed in B^{CN}/B^{CN} mice compared with their wild-type littermates. Other possibilities, which may contribute to these abnormalities, include increased cell death and/or decreased cell proliferation. Terminal deoxynucleotidyl transferase dUTP nick-end labeling assays, however, show no obvious increase in the numbers of apoptotic granule cells in the mutant cerebellum compared with the wild-type sample. Our data, including that from microexplants, are most consistent with a defect in migration of the cerebellar granule cells in B^{CN}/B^{CN} mice. This delayed migration of granule cells can also contribute to the abnormal formation of cerebellar foliation and abnormal dendrite development of the Purkinje cells of these mice. The abnormalities we describe in the cerebellum, together with the absence of the pontine nuclei in their normal location, most likely contribute to the marked ataxia and loss of balance found in the B^{CN}/B^{CN} mice.

Why Are These Particular Neurons Most Affected?

We stained a series of brain sections with antibodies raised against the three NMHC II isoforms and compared the staining of the neurons found to be affected in B^{CN}/B^{CN} mice to the immediate surrounding area. In each case, the affected neurons are more enriched for NMHC II-B than are the surrounding neurons. On the other hand, this is not the case for the inferior olive. Thus, one possible cause for migrational defects in these particular neurons seems to be the predominance of the NMHC II-B isoform. However, work from a number of different laboratories by using cultured cells suggests specific functions for myosin II-A and II-B in a number of different cells (Kolega, 2003; Wylie and Chantler, 2003; Lo *et al*., 2004), so we cannot rule out a role for both the extent of expression and specificity of isoform function in our study. The severity of abnormalities may also differ depending on the complexity of migration. The facial and AES neurons, which follow long and complicated pathways, may be affected more severely than those with less distance to traverse. However, even in these affected neurons migration is not abolished in B^{CN}/B^{CN}, B^{C}/B^{C} and B^{-}/B^{-} mice. All these results suggest that myosin II-B is just one of the motors driving neuronal migration in these three groups of neurons. Figure 8E also shows the dominance of NMHC II-B staining in the Purkinje cells of the cerebellum. This increased staining may not be related to cell migration, but to dendrite formation and maintenance, and/or synaptic formation.

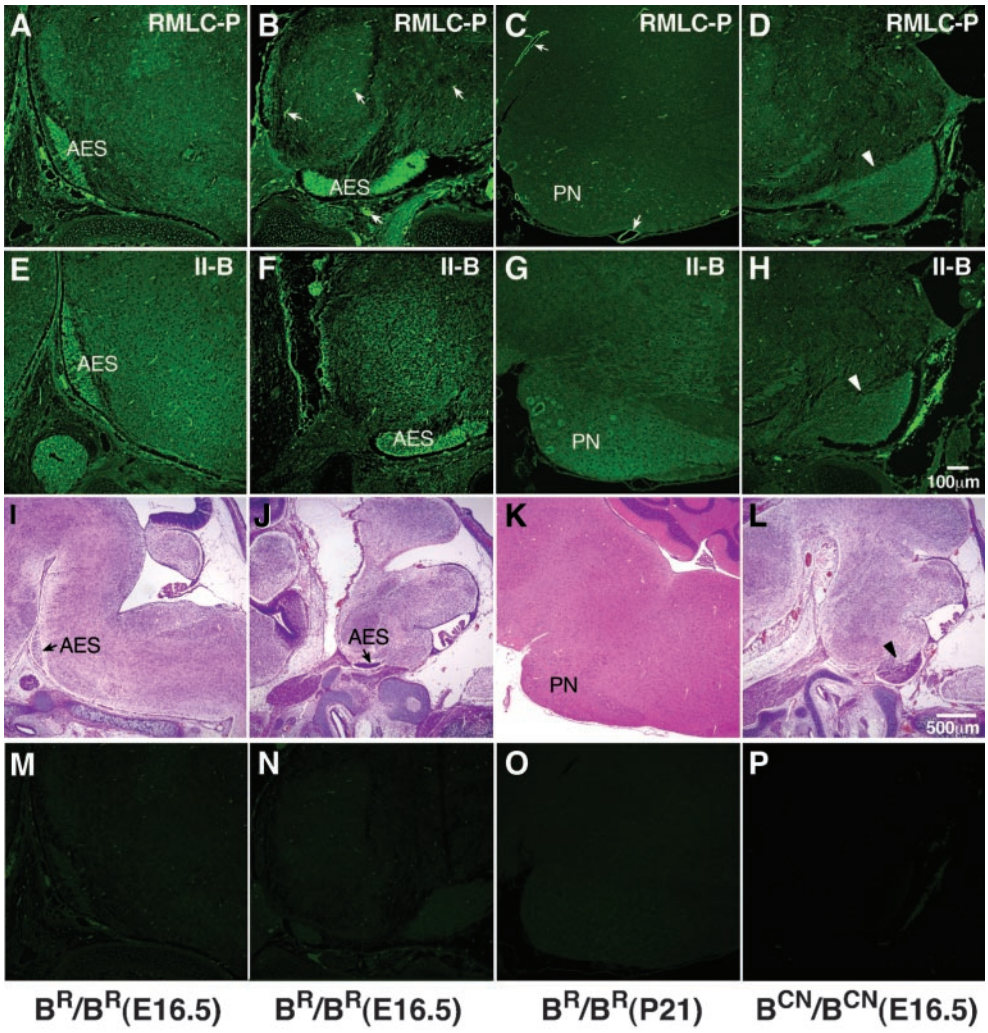

Figure 9. Increased phosphorylation of the RMLC in the AES. (A–D) Immunofluorescence confocal images stained for RMLC-P in the AES, containing migrating pontine neurons (A and B), and stationary pontine neurons (C, PN) in B^R/B^R mice and the abnormally accumulated neurons of the putative AES in B^{CN}/B^{CN} mice (D, arrowhead). At E16.5, the migrating pontine neurons in both medial (A) and lateral (B) sections and the vasculature (B, arrows) show a marked increase in phosphorylation of the RMLC. This increase is not present in stationary pontine neurons at P21, where strong staining remains in the vasculature (C, arrows). In B^{CN}/B^{CN} mice, the migration of the AES is slowed (Figure 5), but the increase in RMLC-P is still observed (D, arrowhead). (E–H) Corresponding sections stained for NMHC II-B. Both the migrating (E and F) and stationary pontine neurons (G) show increased amounts of NMHC II-B compared with the surrounding areas. In B^{CN}/B^{CN} mice, this increase in staining is seen in the mutant putative AES (H, arrowhead). (I–L) H&E staining of the corresponding sections at low magnification to show identification of neurons. (M–P) Negative control for immunofluorescence staining by using normal rabbit IgG as primary antibody.

Phosphorylation of Myosin during Pontine Neuron Migration

Using an antibody specific for the phosphorylated form of Ser-19, we demonstrate that the level of phosphorylated RMLC is significantly elevated in migrating, but not in stationary pontine neurons. Studies from netrin-1 knockout mice and pontine explant cultures demonstrated an important role for netrin-1 signaling through its receptor Deleted in Colorectal Cancer (DCC) in directing neurite outgrowth from pontine neurons (Yee *et al.*, 1999). One possible mechanism for downstream signaling after DCC activation is through the small GTPases Rac1 and Cdc42. Li *et al.* (2002), working with the N1E-115 neuroblastoma cell line, demonstrated that both Rac1 and Cdc42 were activated after netrin-1/DCC signaling and that activation resulted in marked changes in the actin cytoskeleton and promoted neurite outgrowth. Important effectors of Rac1/Cdc42 signaling include a family of homologous serine/threonine kinases, including the p21-activated kinase PAK. In mammalian cells, activation of PAK1 by Rac1/Cdc42 resulted in phosphorylation of Ser-19 on the RMLC (Kiosses *et al.*, 1999; Sells *et al.*, 1999), which is required for nonmuscle myosin II contractile activity. However, activation of PAK was also reported to inhibit myosin light chain kinase and consequently to decrease the phosphorylation of the RMLC (Sanders *et al.*, 1999). Thus, the question of which kinase is actually responsible for the phosphorylation of the RMLC in migrating pontine neurons remains to be resolved. Yee *et al.* (1999) also demonstrated that in cultured pontine neurons, the rate of cell body movement toward the floor plate was significantly decreased in the presence of netrin-1 blocking antibody. Therefore, it seems that netrin-1/DCC is not only signaling the direction of the migration of pontine neurons but also could be signaling the movement of the cell body via activation of myosin II. Whether phosphorylation of myosin plays an important role in regulating the migration of other neurons is not clear at present, because the changes in staining that are observed in the pontine neurons are difficult to discern in migrating facial neurons, although a similar pattern is seen for the cerebellar granule cells (our unpublished data).

Rate-limiting Steps of Neuronal Migration in the Mutant Mice

Like other cells, neurons migrate according to three schematic steps: extension of the leading process in response to the microenvironment, movement of the nucleus toward the leading process (nucleokinesis), and retraction of the tailing process (for review, see Lambert de Rouvroit and Goffinet, 2001). We did not examine whether formation of the leading process is affected in our mutant mice; however, we do not see any obvious differences in the initial formation of the leading process in cerebellar microexplants between the mutant and wild-type mice. Although retraction of the tail

process cannot be ruled out as the rate-limiting step for the defective neuronal migration observed in our mutant mice, it is important to note that some neurons such as the facial neurons and cerebellar granule cells may not retract their tail processes during migration.

Involvement of myosin II in the regulation of nucleokinesis in neural cells has never been directly addressed. Previous work demonstrated that pontine neurons migrate along their long leading process to their destination primarily through nucleokinesis (Yee *et al*., 1999). Delayed migration of the pontine neurons most probably reflects an impairment of nucleokinesis in the mutant mice. Slowed migration of the cerebellar granule cells in the mutant mice may also result from impaired nucleokinesis. This is supported by the following findings from explant culture. 1) No obvious abnormalities in the formation of the leading processes are found in migrating granule cells in the mutant mice compared with their control littermates. 2) Nonmuscle myosin II-B is concentrated in the leading boundary of the nuclei in migrating cells in control animals. In addition, disturbed interkinetic nuclear migration is also observed in the neuroepithelial cells in the mutant mice during neurogenesis (our unpublished data). Based on studies from fish epidermal keratocytes, Svitkina *et al.* (1997) proposed that forward translocation of the cell body (nucleus) was driven by contraction of an actin-myosin II network. Network contraction at the lamellipodia–cell body transition zone, where myosin II was enriched (and "caped" the cell body), resulted in formation of actin-myosin bundles and forward translocation of the cell body. Our results support a similar mechanism for driving neural cell migration in the affected cells described above. We propose that nonmuscle myosin II-B contributes directly to neuronal migration by driving forward nucleus translocation toward the leading process in these cells.

ACKNOWLEDGMENTS

We acknowledge useful discussions with members of the Laboratory of Molecular Cardiology. We are particularly indebted to Drs. Shirley Bayer and Joseph Altman for valuable comments on the manuscript. Chengyu Liu and Yubin Du (National Heart, Lung, and Blood Institute Transgenic Core) and William K. Riemenschneider (Light Microscopy Core) provided outstanding service. Fumio Matsumura (Rutgers University) kindly provided the antibodies to detect phosphorylated Ser-19 on the RMLC. Mary Anne Conti made significant improvements in the manuscript. Catherine Magruder's editorial assistance is also gratefully acknowledged.

REFERENCES

Altman, J., and Bayer, S.A. (1987). Development of the precerebellar nuclei in the rat. J. Comp. Neurol. *257*, 477–552.

Altman, J., and Bayer, S.A. (1997). Development of the cerebellar system in relation to its evolution, structure, and functions, Boca Raton, FL: CRC Press.

Bloch-Gallego, E., Ezan, F., Tessier-Lavigne, M., and Sotelo, C. (1999). Floor plate and netrin-1 are involved in the migration and survival of inferior olivary neurons. J. Neurosci. *19*, 4407–4420.

Brown, M.E., and Bridgman, P.C. (2003). Retrograde flow is increased in growth cones from myosin IIB knockout mice. J. Cell Sci. *116*, 1087–1094.

Buxton, D.B., Golomb, E., and Adelstein, R.S. (2003). Induction of nonmuscle myosin heavy chain II-C by butyrate in RAW 264.7 mouse macrophages. J. Biol. Chem. *278*, 15449–15455.

Crawley, J.N. (2003). Behavioral phenotyping of rodents. Comp. Med. *53*, 140–146.

De Lozanne, A., and Spudich, J.A. (1987). Disruption of the *Dictyostelium* myosin heavy chain gene by homologous recombination. Science *236*, 1086–1091.

Diefenbach, T.J., Latham, V.M., Yimlamai, D., Liu, C.A., Herman, I.M., and Jay, D.G. (2002). Myosin 1c and myosin IIB serve opposing roles in lamellipodial dynamics of the neuronal growth cone. J. Cell Biol. *158*, 1207–1217.

Garel, S., Garcia-Dominguez, M., and Charnay, P. (2000). Control of the migratory pathway of facial branchiomotor neurons. Development *127*, 5297–5307.

Gleeson, J.G., and Walsh, C.A. (2000). Neuronal migration disorders: from genetic diseases to developmental mechanisms. Trends Neurosci. *23*, 352–359.

Golomb, E., Ma, X., Jana, S.S., Preston, Y.A., Kawamoto, S., Shoham, N.G., Goldin, E., Conti, M.A., Sellers, J.R., and Adelstein, R.S. (2004). Identification and characterization of nonmuscle myosin II-C., a new member of the myosin II family. J. Biol. Chem. *279*, 2800–2808.

Hatten, M.E. (1999). Central nervous system neuronal migration. Annu. Rev. Neurosci. *22*, 511–539.

Heath, K.E., *et al.* (2001). Nonmuscle myosin heavy chain IIa mutations define a spectrum of autosomal dominant macrothrombocytopenias: May-Hegglin anomaly and Fechtner, Sebastian, Epstein, and Alport-like syndromes. Am. J. Hum. Genet. *69*, 1033–1045.

Hu, A., Wang, F., and Sellers, J.R. (2002). Mutations in human nonmuscle myosin IIA found in patients with May-Hegglin anomaly and Fechtner Syndrome result in impaired enzymatic function. J. Biol. Chem. *277*, 46512–46517.

Kawamoto, S., and Adelstein, R.S. (1991). Chicken nonmuscle myosin heavy chains: differential expression of two mRNAs and evidence for two different polypeptides. J. Cell Biol. *112*, 915–924.

Kiosses, W.B., Daniels, R.H., Otey, C., Bokoch, G.M., and Schwartz, M.A. (1999). A role for p21-activated kinase in endothelial cell migration. J. Cell Biol. *147*, 831–844.

Kolega, J. (2003). Asymmetric distribution of myosin IIB in migrating endothelial cells is regulated by a rho-dependent kinase and contributes to tail retraction. Mol. Biol. Cell *14*, 4745–4757.

Komuro, H., and Rakic, P. (1996). Intracellular Ca2+ fluctuations modulate the rate of neuronal migration. Neuron *17*, 275–285.

Lambert de Rouvroit, C., and Goffinet, A.M. (2001). Neuronal migration. Mech. Dev. *105*, 47–56.

Li, X., Saint-Cyr-Proulx, E., Aktories, K., and Lamarche-Vane, N. (2002). Rac1 and Cdc42 but not RhoA or Rho kinase activities are required for neurite outgrowth induced by the Netrin-1 receptor DCC (deleted in colorectal cancer) in N1E-115 neuroblastoma cells. J. Biol. Chem. *277*, 15207–15214.

Lo, C.M., Buxton, D.B., Chua, G.C.H., Dembo, M., Adelstein, R.S., and Wang, Y.U. (2004). Nonmuscle myosin IIB is involved in the guidance of fibroblast migration. Mol. Biol. Cell *15*, 982–989.

Matsumura, F., Ono, S., Yamakita, Y., Totsukawa, G., and Yamashiro, S. (1998). Specific localization of serine 19 phosphorylated myosin II during cell locomotion and mitosis in cultured cells. J. Cell Biol. *140*, 119–129.

Phillips, C.L., Yamakawa, K., and Adelstein, R.S. (1995). Cloning of the cDNA encoding human nonmuscle myosin heavy chain-B and analysis of human tissues with isoform-specific antibodies. J. Muscle Res. Cell Motil. *16*, 379–389.

Sanders, L.C., Matsumura, F., Bokoch, G.M., and de Lanerolle, P. (1999). Inhibition of myosin light chain kinase by p21-activated kinase. Science *283*, 2083–2085.

Sells, M.A., Boyd, J.T., and Chernoff, J. (1999). p21-activated kinase 1 (Pak1) regulates cell motility in mammalian fibroblasts. J. Cell Biol. *145*, 837–849.

Sellers, J.R. (1999). Protein profile: myosins, 2nd ed., Oxford, United Kingdom: Oxford University Press.

Serafini, T., Colamarino, S.A., Leonardo, E.D., Wang, H., Beddington, R., Skarnes, W.C., and Tessier-Lavigne, M. (1996). Netrin-1 is required for commissural axon guidance in the developing vertebrate nervous system. Cell *87*, 1001–1014.

Sobeih, M.M., and Corfas, G. (2002). Extracellular factors that regulate neuronal migration in the central nervous system. Int. J. Dev. Neurosci. *20*, 349–357.

Svitkina, T.M., Verkhovsky, A.B., McQuade, K.M., and Borisy, G.G. (1997). Analysis of the actin-myosin II system in fish epidermal keratocytes: mechanism of cell body translocation. J. Cell Biol. *139*, 397–415.

Takeda, K., Kishi, H., Ma, X., Yu, Z.-X., and Adelstein, R.S. (2003). Ablation and mutation of nonmuscle myosin heavy chain II-B results in a defect in cardiac myocyte cytokinesis. Circ. Res. *93*, 330–337.

Tullio, A.N., Bridgman, P.C., Tresser, N.J., Chan, C.-C., Conti, M.A., Adelstein, R.S., and Hara, Y. (2001). Structural abnormalities develop in the brain after ablation of the gene encoding nonmuscle myosin II-B heavy chain. J. Comp. Neurol. *433*, 62–74.

Wylie, S.R., and Chantler, P.D. (2003). Myosin IIA drives neurite retraction. Mol. Biol. Cell *14*, 4654–4666.

Yee, K.T., Simon, H.H., Tessier-Lavigne, M., and O'Leary, D.M. (1999). Extension of long leading processes and neuronal migration in the mammalian brain directed by the chemoattractant netrin-1. Neuron *24*, 607–622.